Transonic Viscid-Inviscid Flow Interaction about a Hemisphere-Cylinder

Tsuying Hsieh*
Arnold Engineering Development Center, Arnold Air Force Station, Tenn.

A wind-tunnel investigation was conducted of the viscous-inviscid interaction flowfield about a hemisphere-cylinder at zero incidence in the Mach number range 0.6-0.9. A nose separation bubble is revealed from analysis of shadowgraphs and surface pressure distributions between Mach numbers 0.7 and 0.9. A multiple shock system consisting of a lambda shape shock and two normal shocks prevails in the flowfield as a result of the viscous-inviscid flow interaction which is strongest at $M_\infty = 0.85$. Velocity field measurements utilizing a laser velocimeter were obtained and analyzed by using the concept of an effective body and the particle dynamics for $M_\infty = 0.85$.

Introduction

IN Refs. 1 and 2, a theoretical and experimental investigation of the flowfield about a hemisphere-cylinder at zero incidence in the transonic and low supersonic freestream Mach number M_∞ from 0.7 to 1.3 is presented. It was found that a strong viscid-inviscid flow interaction with boundary-layer separation at the hemispherical nose occurs at $M_\infty \sim 0.8$, yet for $M_\infty \geq 0.9$ no flow separation was observed. A similar separation phenomenon is also presented in the data of Ref. 3. Since a hemisphere-cylinder is one of the basic nose configurations for blunt nose bodies of revolution, a detailed study of the phenomena of transonic viscid-inviscid flow interaction with boundary-layer separation shall reveal the physical features of transonic axisymmetrical flow over blunt nose bodies in general.

In this paper, an experimental investigation of the viscous-inviscid flow interaction phenomena for a hemisphere-cylinder at Mach numbers from 0.6 to 0.9 is presented. First, a nose separation bubble is revealed from analysis of shadowgraphs and surface pressure distribution between Mach numbers from 0.7 to 0.9. This result indicates a basic difference in the mechanism of separation between the present nose separation and the leading-edge separation of blunt nose airfoils and will be discussed herein. Second, a multiple shock system, consisting of a lambda shape shock and two normal shocks, prevails in the flowfield as a result of the viscid-inviscid flow interaction. The observed nose separation bubble and the multiple normal shocks are also analyzed through inviscid calculation utilizing the concept of an effective body and shown to be physically sound. Third, a velocity field survey was conducted using a laser velocimeter. The influence of the nose separation on the velocity field is presented by comparison of the measured velocity components with the inviscid solutions for the hemisphere-cylinder and the effective body. A particle dynamic analysis to account for the particle lag in LV measurements is also presented.

Test Apparatus

A. Wind-Tunnel Facility and Model

The experiments described herein were performed in the AEDC Aerodynamic Tunnel (1T). This facility is a continuous flow, nonreturn wind tunnel capable of being operated at Mach numbers from 0.2 to 1.5. The test section is 1 ft square and 37.5 in. long with 6% porous walls at the top and bottom and two plexiglas side walls for flow visualization. The model used in the test is a hemisphere-cylinder 1 in. in diameter and 10 in. long and is made of stainless steel. Eighteen pressure orifices are located along a single plane. The model is sting mounted with a sting diameter of 0.75 in.

B. Flow Visualization

Shadowgraphs were taken in this experiment. The shadowgraph system is an off-axis, collimated beam, direct shadowgraph type. An air gap spark is the point light source (effective diameter = 0.04 in.), and it provides exposure of approximately 1 μs duration. The source is positioned at the focus of a 16-in.-diam $f/8$ parabolic mirror. This mirror reflects light from the source in a collimated beam through the wind-tunnel test section, perpendicular to the flow, and directly onto film (11 × 14 in. to cover the field of interest).

C. Laser Velocimeter System

The LV used for the present experiment is a two-component, dual-scatter, Bragg-cell-type system operating in the on-axis, back-scatter collection mode with a 1.5-W argon ion laser.[4] The system is capable of measuring velocity in the range from −152 to 490 m/s for the horizontal component and ±122 m/s for the vertical. The entire optical system is mounted on a 3 axis transverse mechanism with a position resolution accuracy of ±0.0025 cm in all three directions. The scattering source (or tracer particle) is the natural aerosol particles entrained in the flow medium. In order to obtain a sound statistical sample, about 1000 samples were taken in each measurement. The mean value of the samples is used to represent the local flow velocity.

Results and Discussion

A. Flow Separation and Shock System

In Ref. 1, flow separation about a hemisphere-cylinder at zero incidence was observed at $M_\infty = 0.8$. The effect of compressibility on flow separation is presented in this section for $M_\infty = 0.6$-0.9 within a Reynolds number range from 4.2 to 5.1×10^6 per foot. The variation of Reynolds number is negligible in the present experiment. Figure 1 shows the shadowgraph of flow past the hemisphere cylinder for $M_\infty = 0.6$-0.9. At $M_\infty = 0.6$, the flow is well attached and no shock appears. Between $M_\infty = 0.7$ and 0.85, there is flow separation at the nose, a shock system, and reattachment. The

Received Dec. 12, 1976; revision received April 3, 1978.

Index categories: Subsonic Flow; Transonic Flow; Jets, Wakes, and Viscid-Inviscid Flow Interactions.

*Research Engineer, PWT/4T. Member AIAA.

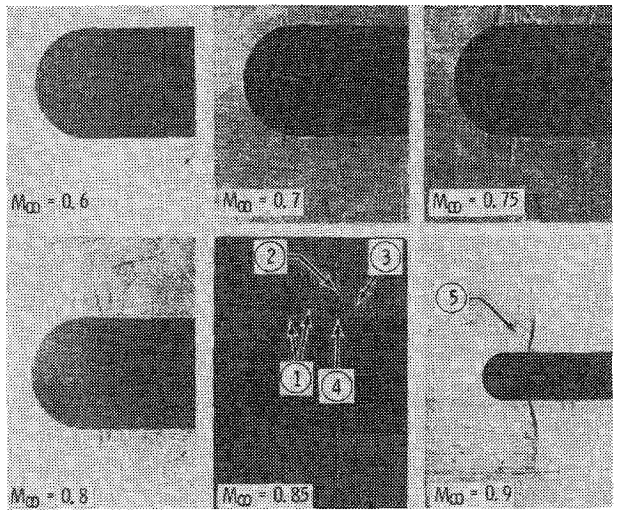

Fig. 1 Shadowgraphs of flow past hemisphere-cylinder at $\alpha = 0$. (1) Lambda shape shock; (2) major normal shock; (3) minor normal shock; (4) separation bubble; (5) recompression shock.

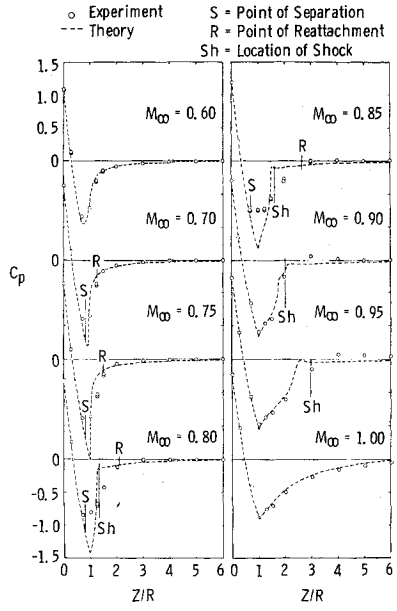

Fig. 2 Comparison of surface pressure between experiments and calculations.

most pronounced separation region occurs at $M_\infty = 0.85$. At $M_\infty = 0.9$ and above,[1] flow separation is not observed, and a well-defined normal shock appears. Therefore, the nose separation bubble occurs for the hemisphere-cylinder at Mach numbers between 0.7 and 0.9.

The relaxation solution of the steady, full potential equation given by Ref. 5 is employed to compute the inviscid flowfield in the present investigation. A comparison of the measured surface pressure with the inviscid theory for $M_\infty = 0.6$-1.0 is shown in Fig. 2. The point of separation, reattachment, and the shock location (only the major normal shock location is shown for multiple shock cases) as estimated from an enlarged version of the shadowgraph of Fig. 1 are also indicated in Fig. 2. The minimum pressure $C_{P_{\min}}$ and the critical pressure C_P^* (supercritical flow prevails when $C_{P_{\min}} < C_P^*$) are plotted as a function of Mach number in Fig. 3. At $M_\infty = 0.6$, the comparison between theory and experiment is satisfactory and the flow is subsonic everywhere ($C_{P_{\min}} > C_P^*$) with $C_{P_{\min}}$ occurring ahead of the junction of the hemisphere and cylinder. For $M_\infty > 0.7$, supercritical flow prevails. From $M_\infty = 0.7$-0.85, poor agreement between theory and experiment is found in the separated region as expected, while in the region of attached flow (downstream) the agreement is again good. For $M_\infty = 0.9$ and above, some difference in surface pressure between theory and experiment also occurs in the region where the deviation of shock location is found (Fig. 2). The discrepancy in shock location may be caused by the interaction between the boundary layer and the shock (without flow separation), which is not treated in the theory. This statement is based on the fact that excellent agreement is shown in the same figure for $M_\infty = 1.0$ without the presence of the shock on the body.

A better understanding of the phenomena of the nose separation bubble and the shock system can now be pursued. The flowfield of the nose separation bubble, as shown in Fig. 1, appears to be similar to the shock-induced leading-edge separation bubble discussed in great detail for blunt nose airfoils.[6] However, there are two basic differences between these types of separation, in that 1) the nose separation bubble presently investigated starts at a point where the pressure ahead of separation is continuously decreasing (Fig. 2) and thus cannot be caused by the boundary-layer separation attributable to reversed pressure gradient, as in the case of leading-edge separation bubble of airfoils; and 2) the appearance and disappearance of nose separation at $M_\infty = 0.7$ and 0.9, respectively, also suggests a basic difference in the mechanism of separation. The mechanism which leads to the separation is argued to be caused by the recompression shock following an overexpansion zone, and the final local flow resembles a supersonic flow over a compression corner. The reason is given as follows. As shown in Fig. 3, the theoretical $C_{P_{\min}}$ value for inviscid flow decreases as Mach number increases from 0.6; $C_{P_{\min}}$ is minimum at $M_\infty = 0.75$ and then increases as Mach number further increases. The $C_{P_{\min}}$ for $M_\infty > 0.6$ occurs at $Z/R = 1$; therefore, the flow at $Z/R < 1$ is under rapid expansion and may be overexpanded, depending on the $C_{P_{\min}}$ value, to cause recompression shock. Such a recompression shock is indicated in the shadowgraphs of Fig. 1 for $M_\infty = 0.9$ without flow separation. When the strength of the recompression shock, which is proportional to $C_{P_{\min}}$, is sufficiently large, the sudden increase in pressure may initiate a flow separation. Once the flow separates, the sudden increase in boundary-layer thickness results in a flow which is similar to supersonic flow (for hemisphere-cylinder, the local flow is supersonic at separation point) over a compression corner, or the so-called viscous ramp, as discussed in Ref. 6 for airfoils with the difference that downstream of the "corner" the surface is curved. Therefore, the interaction of separated flow over a compression corner can describe the local flow. From the preceding argument, a relation can be reached between the flow separation and the $C_{P_{\min}}$ calculated from inviscid theory. A cirtical $C_{P_{\min}}$, or $C_{P_{\min,c}}$ is defined, such that when $C_{P_{\min}} < C_{P_{\min,c}}$ a nose separation bubble is to be expected. The value of $C_{P_{\min,c}}$ for the hemisphere-cylinder is estimated to be approximately -1.20, as shown in Fig. 3. The $C_{P_{\min,c}}$ value may be different for different nose configurations and must be determined empirically. Therefore, it may be interpreted that for $M_\infty \leq 0.6$ or $M_\infty \geq 0.9$, the $C_{P_{\min}}$ value is not sufficiently low to initiate a flow separation at the nose.

The shock system as observed in Fig. 1 contains a lambda shape shock located immediately at the starting point of nose separation bubble or "corner" and two normal shocks (the major and the minor, see Fig. 1 for $M_\infty = 0.8$ and 0.85 for example). The appearance of the lambda shape shock with a forward limb and a very weak rear limb is indeed similar to shock observed in the separated flow over a compression corner and thus is a direct result of the nose separation bubble. The two normal shocks following the lambda shape shock are a result of the curved surface generated by the reattachment of the nose separation bubble and will be demonstrated to be physically sound in the next section. Two interesting points can be made since the reattachment of the

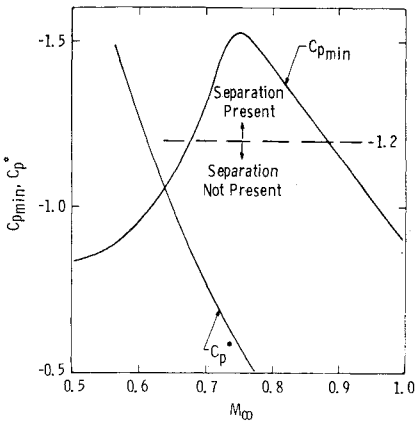

Fig. 3 Minimum pressure and critical pressure as a function of Mach number for hemisphere-cylinder.

bubble occurs only after the appearance of the normal shocks. First, the flow in the downstream vicinity of the lambda shape shock is supersonic; therefore a rapid reattachment is not possible and the bubble height is increasing (see discussion of Ref. 6, pp. 1197-1199). Second, the argument of Ref. 6 that the reattachment of the bubble over a curved surface can only be reached in the region where subsonic flow is re-established also holds in the present investigation. Further illustration of the preceding discussion may be found in the following section.

B. Analysis of Viscous-Inviscid Flow Interaction at $M_\infty = 0.85$

As shown in Fig. 1, a strong viscous-inviscid flow interaction is found for $M_\infty = 0.85$. The questions of interest are: 1) What is the size of the nose separation bubble?; 2) Is the multiple normal shock in the shadowgraph real?; and 3) How much is the external inviscid flowfield influenced by the flow separation? To answer these questions, a velocity measurement using the LV and a theoretical analysis using the concept of effective body are presented in this section. The velocity measurement using the LV for this type of flow is unique because the flowfield is very sensitive to disturbance of any material probe. However, the LV system measures the velocity of the tracer particles entrained in the flow medium rather than the gas velocity itself. In general, there is a difference between the particle velocity and the gas velocity, so-called "particle lag." The particle lag in the AEDC Aerodynamic Wind Tunnel (IT) has been analyzed[7] and is applied herein to the theoretical flowfield computed for the effective body in order to compare with the LV data.

Velocity Distribution

The measured U and V components (mean value from LV samplings) for flow about the hemisphere-cylinder at $M_\infty = 0.85$ are shown in Fig. 4 along the stagnation streamline $Y/R = 0$ and along the radial direction at various stations Z/R from -1 to 6.0. Also shown in Fig. 4 in the solid line is the results of the inviscid theory for the hemisphere-cylinder. The agreement between theory and experiment is fairly good for the region $Z/R \leq 0.4$, where the flowfield is considered to be free from viscous effects. (Note: The agreement between theory and experiment is excellent when the particle lag is taken into account as shown by the dash-and-dot curve in Fig. 4, as will be discussed later.) The interaction region with flow separation previously observed in the shadowgraph extends from $Z/R = 0.7$-3.0 approximately. It can be seen that the velocity predicted by inviscid theory differs significantly from the experiment in this region also. For $Z/R \geq 3.0$, a thick boundary layer is indicated by experimental results.

LV measurements inside the separation bubble were not satisfactory because of the type of nose or leading-edge separation encountered. As shown in Ref. 8, the majority of

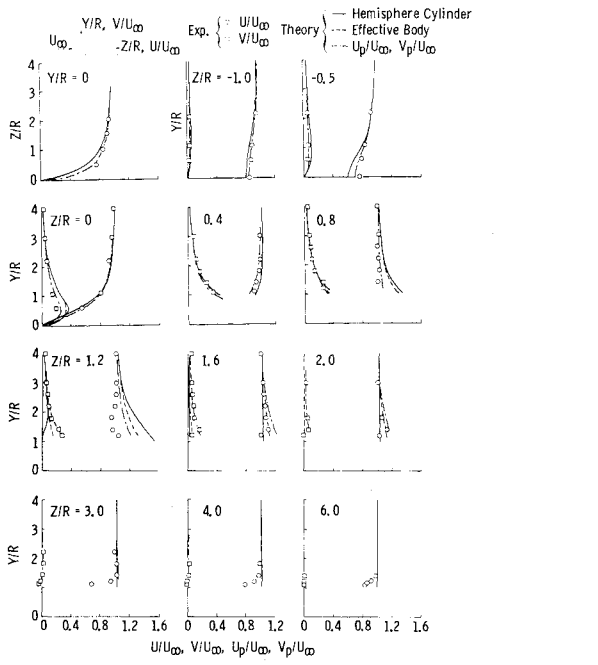

Fig. 4 Velocity field about hemisphere-cylinder at zero incidence and $M_\infty = 0.85$.

tracer particles in the separated region do not follow the gas. Tracer particles with inertia may penetrate through the separated region. Only particles sufficiently small in size would follow the streamlines and not enter the separated region (a reduction of data rate in the separated region was distinctly indicated). Some of the small particles may enter the separated region at the reattachement location, and these trapped particles can follow the gas even in the separated region. The evidence is that in the LV samples obtained in the separated region show simultaneous positive (about 183 m/s) and negative (as large as -107 m/s) velocities with about 15% or less in total samples for the latter. Such sampled results confirm that the flow is indeed separated, otherwise no negative velocity samples can possibly be detected, but the local velocity cannot be very well represented because of the large number of particles penetrating the bubble by inertia. Hence, no data in the separated region are presented.

Effective Body

An exact analysis of the interaction region requires solution to the viscous equations. However, a simple analysis for the external inviscid flow only and the approximate size of the separated region may be accomplished by using the concept of effective body.

An effective body is defined to be a body that will give the measured surface pressure of the hemisphere-cylinder. To do this, the computer program used in obtaining inviscid flowfield for pressure curves as shown in Fig. 2 was modified† for the purpose of constructing the effective body. The scheme used is one of trial and error. The body shape was gradually adjusted to obtain the required surface pressure distribution. In the course of the trial-and-error process, it was found that specifying the body curvature and integrating for the body shape would speed up the convergence of the surface pressure. The resulting effective body is shown in Fig. 5. A satisfactory comparison of the computed surface pressure for the effective body with the experimental data is shown in Fig. 6. A plot of curvature distribution for the effective body is included in Fig. 6. Also shown in Figs. 5 and 6

†After the completion of this study, the author became aware of the work of Ref. 9 which can compute the flowfield for bodies with discrete input points for body geometry.

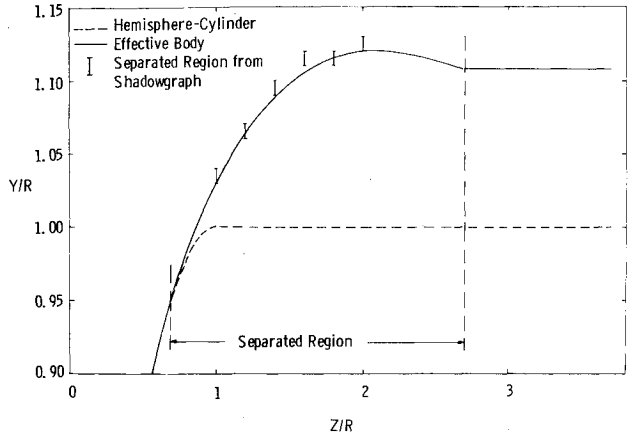

Fig. 5 Comparisons of the calculated effective body with shadowgraph at $M_\infty = 0.85$.

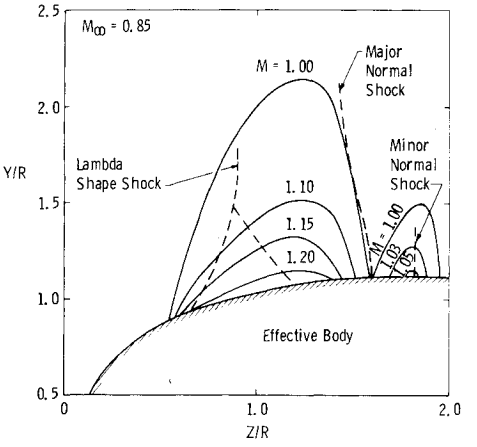

Fig. 7 Mach number distribution in the external flowfield of the effective body.

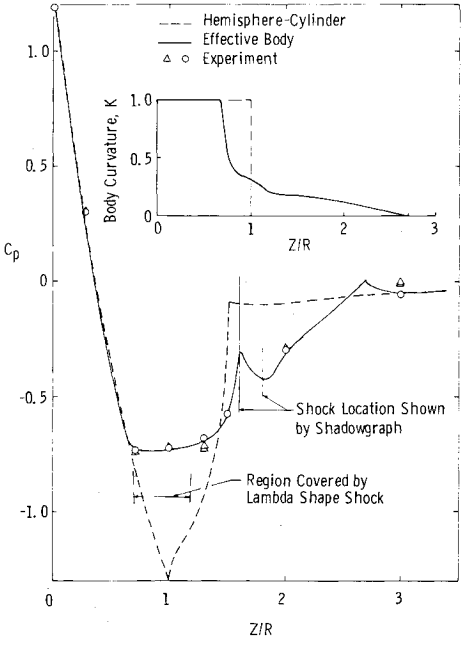

Fig. 6 Surface pressure and curvature distribution over effective body at $M_\infty = 0.85$.

are the inviscid results for the hemisphere cylinder (dash curve) for comparison. To determine the precise shape of separated region from the shadowgraph is difficult, but an approximate estimation can be made, as shown in Fig. 5, and is seen to be comparable to the shape of computed effective body in the fore portion.

It is interesting to point out that a decrease in the thickness of the profile from distance $Z/R > 2.0$ for the effective body (Fig. 5) is necessary in order to match the experimental pressure data at $Z/R = 2.0$ (Fig. 6). This also confirms the bubble-type separation with flow reattachment. The choice of $Z/R = 2.7$ for the end of curved body (Fig. 5) was made to match the experimental pressure data at $Z/R = 3.0$ (Fig. 6), which also agrees with the pressure curve for the hemisphere cylinder. Downstream of $Z/R = 2.7$, the body is approximated by a cylinder 11% larger in radius to simulate the thick boundary-layer development after flow reattachment. This approximation is justified since the pressure for $Z/R \geq 2.7$ is very near the freestream pressure and is not important to the present study. In Fig. 6, the appearance of an expansion followed by a compression resulting in a hump in the surface pressure curve is a result of the flow reattachment.

A plot of the Mach number distribution in the external field for the effective body is shown in Fig. 7. The corresponding shock locations for the lambda shape shock and the major and minor normal shocks, as seen from the shadowgraph, are also plotted in Fig. 7. It is interesting to note that there are two supersonic pockets given by the effective body corresponding to the major and minor normal shocks, respectively, as observed. The exact location of the shocks is generally not given by the theory because of the lack of a shock-fitting scheme in the numerical computation. (In Ref. 5, however, the shock location is represented by the sonic location for the hemisphere-cylinder with a single normal shock, and the predicted shock location is found to be slightly ahead of the experimentally observed one.) The significance of the appearance of the second supersonic pocket is that the observed minor shock is physically possible. This is considered to be a fruitful result of using the effective body to analyze the flowfield. The location for the lambda shape shock is inside the first supersonic pocket as is consistent with the nature of an oblique shock.

Now, a comparison can be made between the velocity field, as predicted by the effective body and the experiments. The comparison is also shown in Fig. 4 by the dash curve. In the regions $Z/R \leq 0.4$ and $Z/R \geq 3.0$, no significant change is shown between the results for the effective body (dash curve) and that for the hemisphere-cylinder (solid curve); this indicates that the influence of flow separation has a negligible effect on the velocity distribution in these two regions. In the interaction region, $0.8 \leq Z/R \leq 2.0$, however, the dash curve at all stations shown more correctly matches the experimental data. In addition, in order to account for the particle lag, an effective particle with radius of 1.37 μm and density of 0.8 g/cm^3 (Ref. 7) was used to compute the particle velocity components U_p and V_p in the external flowfield associated with the effective body, and results are also plotted in Fig. 4 by the chain (dash and dot) curve. The surprisingly good agreement between the chain curve and the experimental data for stations at $Z/R \leq 0.8$ indicates that the flowfield is well represented by the effective body for $Z/R \leq 0.8$. For the station at $Z/R = 1.2$, it is interesting to notice that the U_p component does not agree satisfactorily with the data, but the comparison for the V_p component is surprisingly good. Such a result can be reasoned by the fact that the shock system in the flowfield under investigation is not very well computed by the theory, as discussed in the last paragraph, and these shocks generally have negligible influence on the V component of the gas velocity. In the interaction zone ($1.2 \leq Z/R \leq 2.0$), the U component predicted by the theory is slightly large. The lambda shock starts at about $Z/R = 0.7$, hence for region $Z/R \leq 0.8$ the U_p, V_p are not yet affected by the shocks and good comparisons are expected.

Conclusions

1) A nose separation bubble is found to exist on the fore portion of the hemisphere-cylinder in the Mach number range 0.7 to 0.9, where the minimum local surface pressure from inviscid theory is lower than the critical pressure coefficient of -1.20. The separation is caused by the recompression shock following an expansion zone and the final local flowfield resembles a supersonic flow over a compression corner or visous ramp. The viscous-inviscid flow interaction is found to be most strong at $M_\infty = 0.85$.

2) A multiple shock system is observed as a result of flow separation. The shock system consists of a lambda shape shock and major and minor normal shocks.

3) At $M_\infty = 0.85$, an analysis using the concept of effective body can verify the flowfield as observed from the shadowgraphs for the following interesting points: a) the approximate size of the bubble, b) two supersonic pockets corresponding to the major and minor normal shocks, and c) the influence on the external velocity field as a result of the viscous-inviscid flow interactions.

Acknowledgments

The research reported herein was conducted by the Arnold Engineering Development Center (AEDC), Air Force Systems Command (AFSC). Research results were obtained by personnel of ARO, Inc., contract operator at AEDC. Further reproduction is authorized to satisfy the needs of the U.S. Government.

References

[1] Hsieh, T., "Hemisphere-Cylinder in Transonic Flow, $M_\infty = 0.7 \sim 1.0$," *AIAA Journal*, Vol. 13, Oct. 1975, pp. 1411-1413.

[2] Hsieh, T., "Hemisphere-Cylinder in Low Supersonic Flow," *AIAA Journal*, Vol. 13, Dec. 1975, pp. 1551-1552.

[3] Rogers, E. W. E. and Hall, I. M., "Wall Interference at Transonic Speeds on a Hemisphere-Cylinder Model," Aeronautical Research Council C.P. 510, Sept. 1959.

[4] Lo, C. F., "Transonic Flow Field Measurements Using a Laser Velocimeter," Symposium on Laser Anemometry, University of Minnesota, Oct. 1975.

[5] South, J. C. and Jameson, A., "Relaxation Solutions for Inviscid Axisymmetric Transonic Flow over Blunt or Pointed Bodies," *Proceedings of AIAA Computational Fluid Dynamics Conference*, July 1973, pp. 8-17.

[6] Pearcey, H. H., "Shock Induced Separation and Its Prevention by Design and Boundary Layer Control," *Boundary Layer and Flow Control*, Pergamon Press, Vol. 2, 1961, pp. 1177-1200.

[7] Hsieh, T., "Analysis of Velocity Measurements about a Hemisphere-Cylinder Using a Laser Velocimeter," *Journal of Spacecraft and Rockets*, Vol. 14, May 1977, pp. 280-283.

[8] Hsieh, T., "An Investigation of Separated Flow About a Hemisphere-Cylinder at 0– to 19-deg Incidence in the Mach Number Range from 0.6 to 1.5," AEDC-TR-112, July 1976.

[9] Keller, J. D. and South, J. D., "RAXBOD: A Fortran Program for Inviscid Transonic Flow over Axisymmetric Bodies," NASA TM X-72831, Feb. 1976.